Indian J Phys (October 2015) 89(10):1051–1058
DOI 10.1007/s12648-015-0682-z

ORIGINAL PAPER

Dispersion of electronic bands in intermetallic compound LiBe and related properties

A H Reshak[1,2]*

[1]New Technologies - Research Centre, University of West Bohemia, Univerzitni 8, 306 14 Pilsen, Czech Republic

[2]Center of Excellence Geopolymer and Green Technology, School of Material Engineering, University Malaysia Perlis, 01007 Kangar, Perlis, Malaysia

Received: 09 December 2014 / Accepted: 03 March 2015 / Published online: 4 April 2015

Abstract: Based on the all-electron full-potential linearized augmented plane wave within density functional theory calculations dispersion of the electronic band structure, total and the angular momentum resolved projected density of states, the shape of Fermi surface, the electronic charge density distribution and the optical response of the intermetallic LiBe compound are performed. Seeking the influence of the different exchange correlations on the ground state properties of the intermetallic LiBe, calculations are performed within four types of exchange correlations, namely the local density approximation, general gradient approximation, Engel–Vosko generalized gradient approximation and the modified Becke–Johnson potential. It has been found that replacing the exchange correlations exhibit insignificant influence on the bands dispersion, density of states and hence the optical properties. The obtained results suggest that there exists a strong hybridization between the states resulting in covalent bonds. The Fermi surface is formed by two bands and the center of the Fermi surface is formed by holes. The electronic charge density distribution confirms that the charge is attracted toward Be atoms and the calculated bond lengths are in good accordance with the available experimental data. To get deep insight into the electronic structure, the optical properties are investigated and analyzed in accordance with the calculated band structure and the density of states.

Keywords: LiBe; Intermetallic compound; Electronic band structure; Fermi surface; Electronic charge density distribution

PACS Nos.: 71.15.Mb; 71.20.-b

1. Introduction

The interaction between lithium and beryllium, which are the lightest elemental metallic solids, has been studied with a view to unravel bonding trends and formation of dimmers [1–3]. Jones [4] has calculated the binding energy curves for the 2Sigma+ and 2Pi states of LiBe, LiMg and LiCa using the density functional theory (DFT). Xu et al. [5] have investigated the electronic, vibrational and superconducting properties of LiBe alloy in the $P2_1/m$ structure under pressure using first-principle calculations. Recently, Galav et al. [6] have performed an ab initio calculations using CRYSTAL package within the local density approximation (LDA) and gradient approximation (GGA) to study structural and electronic properties of LiBe. They have reported the bulk modulus, lattice parameters and pressure derivative of the bulk modulus of LiBe compound. Feng et al. [7] have studied the emergent reduction in electronic state dimensionality in dense ordered LiBe alloys, by using VASP code within GGA. They have calculated the static-lattice internal energies of both Be–Li-ordered alloys and the elements at given densities. Fischer et al. [8] have calculated the electric-dipole, potential energy and electronic transition moment functions from highly correlated multireference configuration interaction (MRCI) electronic wave-functions for low-lying doublet and quartet states of the simplest heteronuclear metal diatomic, LiBe and the isoelectronic ion Be_2^+. Also they have calculated the ground state of LiBe, which has been

*Corresponding author, E-mail: maalidph@yahoo.co.uk

found to be bound by 0.31 eV. They have reported that the MRCI values for the equilibrium bond length are about 2.619 Å, which agrees well with the experimental value (2.59 Å). Ling et al. [9] have performed DFT calculation to study the equilibrium geometry and the electronic properties of Be_n and $LiBe_n$ clusters.

It is clear from the above that there exist a number of band structure calculations for LiBe compound using different methods. We have noted that all the calculations are based on non-full potential methods. It would, therefore, seem a natural extension to do more accurate calculations based on full-potential methods. Therefore, we have addressed ourselves for comprehensive theoretical calculations based on the DFT within all-electron full-potential method to calculate the electronic band structure, electronic charge distribution, total and the angular momentum resolved projected density of states (DOS), Fermi surface and the optical properties for LiBe compound. The investigation of the optical properties brings deep insight to understand the origin of the electronic band structure. Therefore, we are interested to calculate the optical properties of the investigated compound. The calculations are performed using four exchange correlation potentials in order to ascertain the effect of exchange correlation on the electronic structure and hence the optical properties. In this calculation, we have employed the state-of-the-art all-electron full-potential linear augmented plane wave (FPLAPW) method, which has proven to be one of the most accurate methods for the computation of the electronic structure of solids within DFT [10–15].

2. Details of calculations

This work was devoted to study the interaction between lithium and beryllium. LiBe crystallizes in monoclinic space group $P2_1/m$. The lattice constants are $a = 1.898$ Å, $b = 3.204$ Å and $c = 4.041$ Å, the unit cell contains four atoms [7]. In the unit cell, Li atom was situated at (0.49797, 0.75000, 0.12165) and Be at (0.19160, 0.75000, 0.60034) with $\alpha = \gamma = 90°$ and $\beta = 80.50°$ [7]. In Fig. 1, we illustrated the crystal structure of the intermetallic compound LiBe. To investigate the ground state properties of LiBe compound, the state-of-the-art all-electron full-potential linear augmented plane wave (FPLAPW) method as implemented in WIEN2k code [16] within DFT was employed. Using GGA [17], we relaxed the geometry by minimizing the forces acting on each atom. We assumed that the structure was totally relaxed when the forces on each atom reached values <1 mRy/a.u.

Form the relaxed geometry, we calculated the ground state properties of LiBe compound. The exchange–correlation potential was solved using the LDA [18] and GGA,

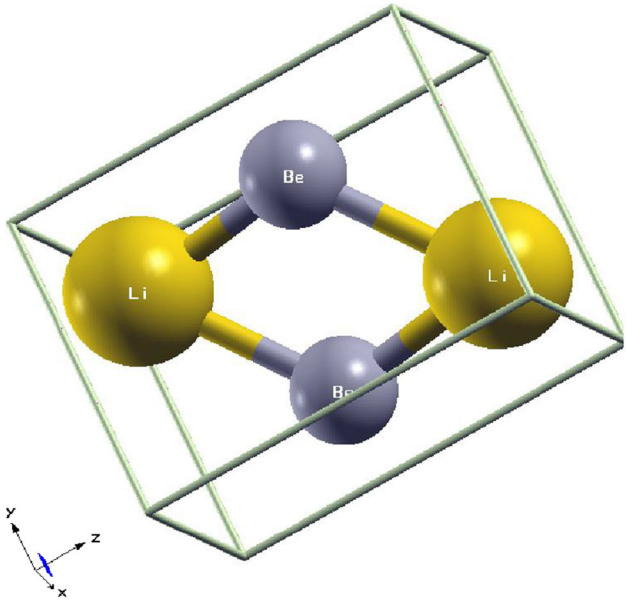

Fig. 1 Fragment of the crystal structure of intermetallic LiBe compound

which were based on exchange–correlation energy optimization to calculate the total energy. In additional, we used Engel–Vosko generalized gradient approximation (EV-GGA) [19], which was able to reproduce better exchange potential at the expense of less agreement in the exchange energy. This approach yielded better band splitting compared to LDA and GGA. For better results, we used the recently modified Becke–Johnson potential (mBJ) [20], which optimized the corresponding potential for electronic band structure calculations. To solve the Kohn–Sham equations, a basis of linear APW's was used. In the muffin-tin (MT) spheres, the potential and charge density were expanded in spherical harmonics with $l_{max} = 8$ and nonspherical components up to $l_{max} = 6$. In the interstitial region, the potential and the charge density were represented by Fourier series. Self-consistency was obtained using 200 $\vec{k}$ points in the irreducible Brillouin zone (IBZ). The self-consistent calculations were converged since the total energy of the system was stable within 10^{-5} Ry.

3. Results and discussion

3.1. Electronic band structure dispersion and density of states

The electronic band structure along the high symmetry directions $\Gamma \to Y \to C \to Z \to \Gamma \to B \to D$ of the monoclinic structure [21] for the intermetallic compound LiBe is investigated using four types of exchange–correlation potentials namely LDA, GGA, EVGGA and mBJ.

We would like to mention here that in our previous works [22–25], we have calculated the electronic stature, linear and nonlinear optical susceptibilities using FPLAPW method within mBJ on several systems, whose electronic structure, linear and nonlinear optical susceptibilities are known experimentally. In those previous calculations, we have found very good agreement with the experimental data. Thus, we believe that our calculations reported in this paper within mBJ, would produce very accurate and reliable results. Therefore, we present only the results obtained from mBJ as illustrated in Fig. 2(a). Figure 2(b) exhibits the Brillouin zone of LiBe. It is clear that moving from LDA → GGA → EVGGA → mBJ shows insignificant influence on the bands dispersion. In all cases, we have found that there are two bands cross-Fermi level along the directions $\Gamma \rightarrow Y \rightarrow C \rightarrow Z$ and $\Gamma \rightarrow B \rightarrow D$ of the symmetry points of BZ. In general, our calculated electronic band structure shows reasonable agreement with that obtained by Galav et al. [6]. The similar features are also observed by Xu et al. [5] at 80 and 100 GPa in monoclinic LiBe. Our calculation show that the top of the valence band is about 5.0 eV above E_F in reasonable agreement with previous result [6].

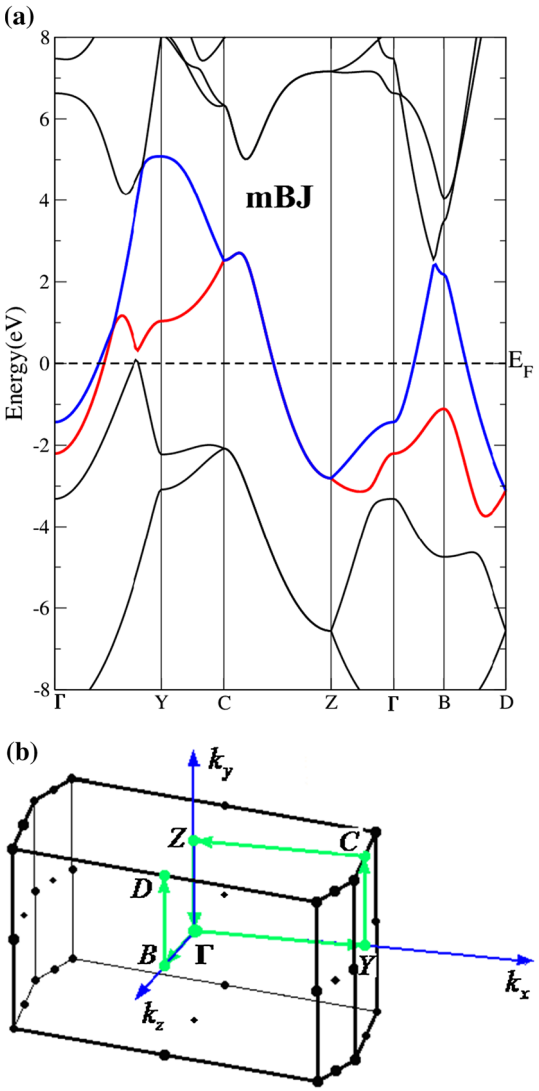

Fig. 2 The calculated electronic band structure of intermetallic LiBe compound using four exchange correlation potentials (LDA, GGA, EVGGA, mBJ); (**a**) The results obtained from mBJ along the high symmetry directions the *red* and *blue colors* just to highlight the bands which cross the Fermi level and (**b**) Brillouin zone of LiBe

In order to inspect the hybridization and the types of orbitals, which control the overlapping around Fermi level, we investigate the total and the angular momentum resolved projected DOS for LiBe compound. In the DOS calculation, the step size (dE) is taken to be 0.002. The total DOS are plotted using four types of the exchange–correlation potentials, which confirm our previous observation that there is insignificant influence, when we move from LDA → GGA → EVGGA → mBJ as represented in Fig. 3(a). Therefore, we select to show the mBJ results to represent the partial DOS as shown in Fig. 3(b). The calculated partial DOS exhibits that Be-*s*/*p* and Li-*s*/*p* states control the overlapping around Fermi level. The DOS at Fermi level $N(E_F)$ is determined by the overlap between these states. The values of $N(E_F)$ for the total and partial DOS are listed in Table 1, which show that $N(E_F)$ of Be-$p > N(E_F)$ of Li-$p > N(E_F)$ of Li-s $> N(E_F)$ of Be-s. These values suggest that the overlapping is strong enough, indicating that the metallic nature of the investigated compound and Be atom shows the highest DOS at the Fermi energy compared to Li atom in good agreement with the previous work of Galav et al. [6] and Feng et al. [7]. Using the existing values of $N(E_F)$, one can obtain the electronic specific heat coefficient (γ), which can be determined by using the expression,

$$\gamma = \frac{1}{3}\pi^2 N(E_F) k_B^2, \tag{1}$$

where $N(E_F)$, is the DOS at Fermi energy and k_B is the Boltzmann constant. The calculated γ for the total and partial DOS are listed in Table 1, which shows that γ of Be-$p > \gamma$ of Li-$p > \gamma$ of Li-s $> \gamma$ of Be-s is in consistence with the values of $N(E_F)$.

The calculated partial DOS enables us to identify the angular momentum character of the various structures and the overlapping around Fermi level. The Fermi level is situated at 0.0 eV. Following Fig. 3(b), one can see that below Fermi level, in the energy range between −9.0 up to −6.0 eV, there exists a strong hybridization between Li-*s* and Li-*p* states, whereas above the Fermi level, Li-*p* exhibits a strong hybridization with Be-*p* state. In the energy region between 2.0 and 4.0 eV, Li-*s* state hybridizes with Be-*s* state. We would like to mention that the strong hybridization may lead to covalent bonds between the atoms.

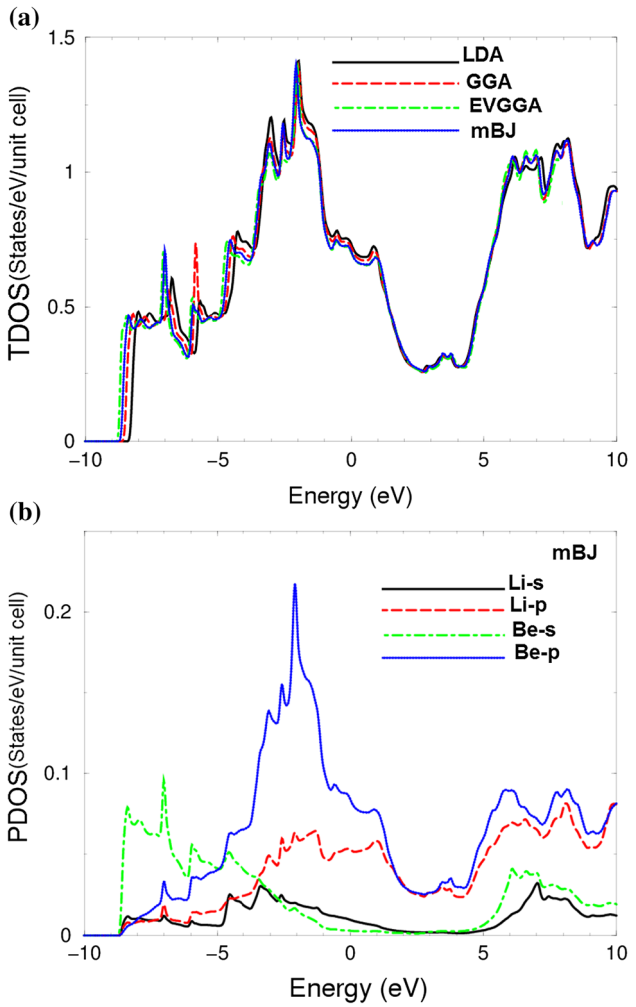

Fig. 3 (**a**) Calculated total density of states using LDA, GGA, EVGGA and mBJ; (**b**) calculated partial density of states Li-*s*/*p* and Be-*s*/*p* using mBJ

The partial DOS extending from −8.0 eV up to Fermi level exhibits that Be-*p* state posseses the highest contribution (0.22 electron/eV), then Be-*s* state (0.1 electron/eV), Li-*p* state (0.06 electron/eV) and Li-*s* state (0.02 electron/eV), indicating that there are some electrons from Li-*s*/*p* and Be-*s*/*p* are transferred into valence bands and contribute to covalence interactions due to the strong hybridization between the states. To support this statement, we have taken a deep careful look at electronic charge density distribution of LiBe, which are plotted in (1 0 0) and (1 0 1) crystallographic planes in Fig. 4(a) and 4(b). It is clear that Li atom surrounding by red area, indicating that (according to the thermoscale) there is a zero charge around this atom, while there is green area surrounding Be atom indicating partial charges accumulated around Be atom. According to the nuclear charge for Be (+4e) and Li (+3e), the 1 s core of Be atom has small spatial extent than that of Li and from the electro-negativity difference between Li (0.98) and Be (1.57), one can see that the charge is attracted toward Be atoms, which is clearly shown by the red (0.0000) and green (0.6000) colors according to charge density scale corresponds to the maximum charge accumulation site. The calculated distance between Li–Be atoms is about 2.55 Å, which agrees well with the experimental value (2.59 Å) [26] and the previous theoretical results 2.545 Å [27], 2.619 Å [26] and 2.607 Å [28].

Table 1 Calculated density of states at Fermi level $N(E_F)$ for LiBe, Li-*s*/*p* and Be-*s*/*p* states along with the calculated electronic specific heat coefficient (γ)

$N(E_F)$	LDA	GGA	EVGGA	mBJ
$N(E_F)$@LiBe (states/Ry/cell)	10.05	9.86	9.63	9.62
$N(E_F)$@Li-*s* (states/Ry/cell)	0.14	0.13	0.13	0.13
$N(E_F)$@Li-*p* (states/Ry/cell)	0.75	0.72	0.68	0.72
$N(E_F)$@Be-*s* (states/Ry/cell)	0.04	0.04	0.04	0.04
$N(E_F)$@Be-*p* (states/Ry/cell)	1.25	1.22	1.17	1.15
γ@LiBe (mJ/mole-K^2)	1.74	1.71	1.67	1.66
γ@Li–s (mJ/mole-K^2)	0.02	0.02	0.02	0.02
γ@Li-*p* (mJ/mole-K^2)	0.13	0.12	0.12	0.13
γ@Be-*s* (mJ/mole-K^2)	0.01	0.01	0.01	0.01
γ@Be-*p* (mJ/mole-K^2)	0.22	0.21	0.20	0.20

3.2. Fermi surface

Based on the calculated electronic band structure, there are two bands crossing Fermi level, which forms the shape of Fermi surface for LiBe compound. The Fermi level is determined via the Kohn–Sham eigenvalue of the highest occupied state. The shape of Fermi surface is represented in Fig. 5(a)–5(c). Figure 5(a) and 5(b) represent Fermi surface's shape formed by band number 5 and 6, respectively, which consists of the partial DOS at Fermi level, whereas Fig. 5(c) exhibits the shape of Fermi surface, which consist of empty areas that represent the holes and shaded areas corresponding to the electrons. It is clear that at the center of Brillouin zone, the Fermi surface is shaped from holes, whereas the Fermi surface at the other symmetry directions is shaped from both of holes and electrons. The shape of Fermi surface helps to predict the magnetic, electrical, thermal and optical properties of the metallic and semimetallic materials.

3.3. Optical properties

The calculations of the optical dielectric function involve the energy eigenvalues and electron wave-functions, which are natural outputs of band structure calculations. Since LiBe crystallizes in monoclinic structure, there are only five nonzero components of the optical dielectric tensors,

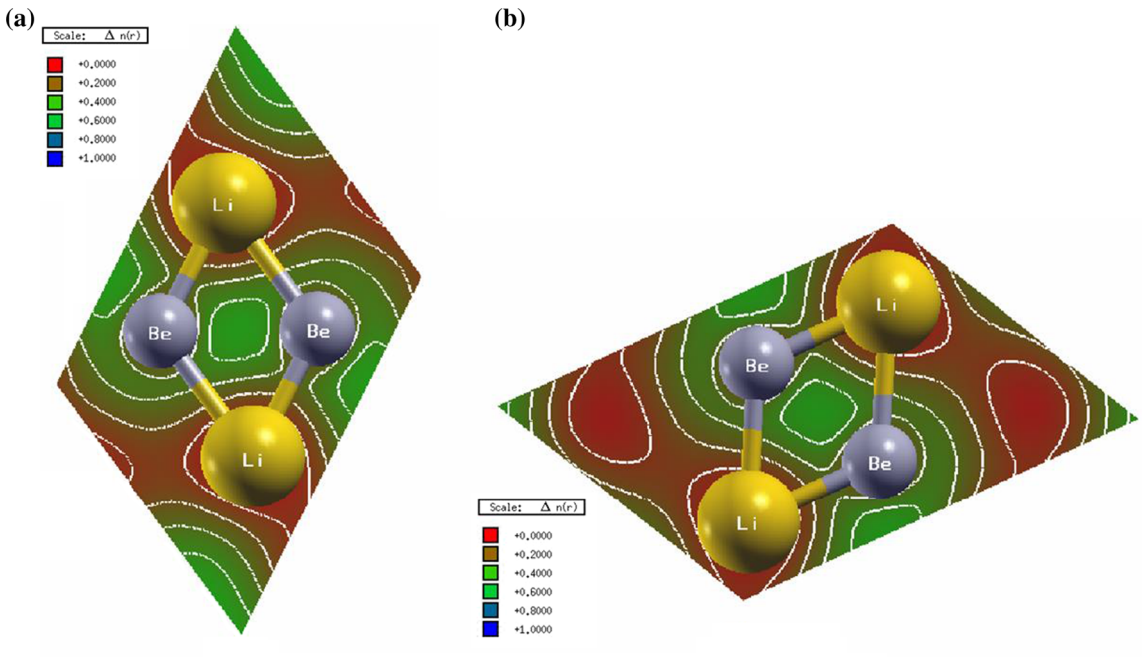

Fig. 4 The electron charge density distribution was calculated for; (**a**) (1 0 0) crystallographic plane and (**b**) (1 0 1) crystallographic plane

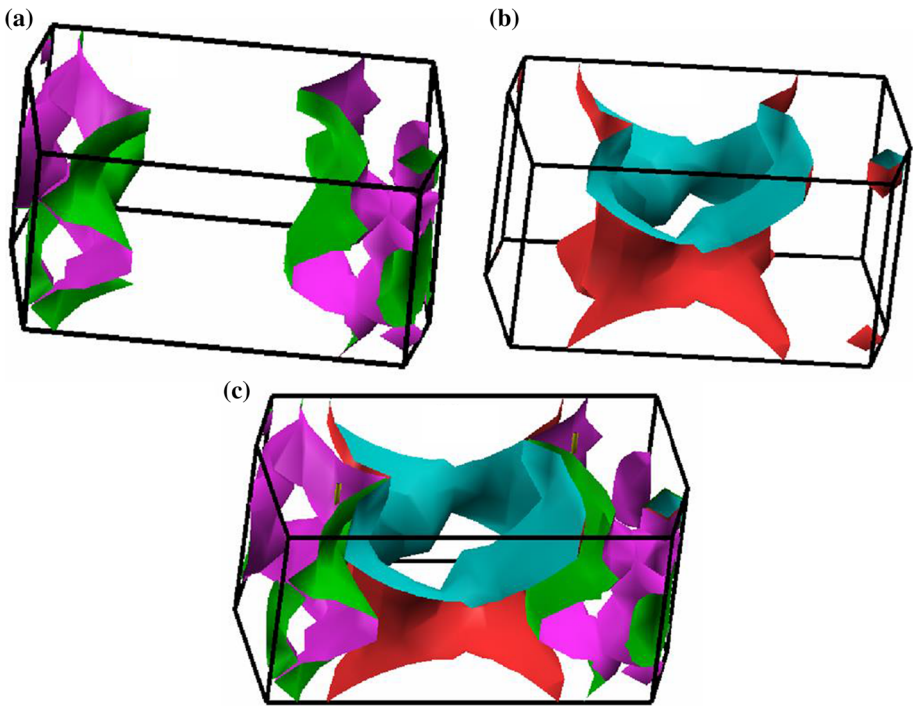

Fig. 5 Calculated Fermi surface; (**a**) for band # 5; (**b**) for band # 6; (**c**) for shape of Fermi surface

which completely characterize the linear optical properties. We have concentrated only on the major components, corresponding to an electric field perpendicular and parallel to the **c**-axis. The corresponding optical dielectric functions are $\varepsilon^{xx}(\omega)$, $\varepsilon^{yy}(\omega)$ and $\varepsilon^{zz}(\omega)$. The imaginary parts $\varepsilon_2^{xx}(\omega)$, $\varepsilon_2^{yy}(\omega)$ and $\varepsilon_2^{zz}(\omega)$ representing dispersion of the optical function are calculated using the following expression [29]:

$$\varepsilon_2^{ij}(\omega) = \frac{8\pi^2\hbar^2e^2}{m^2V}\sum_k\sum_{cv}(f_c - f_v)\frac{p_{cv}^i(k)p_{vc}^j(k)}{E_{vc}^2} \times \delta[E_c(k) - E_v(k) - \hbar\omega] \quad (2)$$

where m, e and $\hbar$ are the electronic mass, electronic charge and Planck's constant, respectively. f_c and f_v represent the Fermi distributions of the conduction and valence bands,

Table 2 The calculated ω_P^{xx}, ω_P^{yy} and ω_P^{zz} when $\varepsilon_1^{xx}(\omega)$, $\varepsilon_1^{yy}(\omega)$ and $\varepsilon_1^{zz}(\omega)$ cross-zero

xc	ω_P^{xx}	ω_P^{yy}	ω_P^{zz}
LDA	9.199	8.860	6.445
GGA	9.274	8.922	6.526
ECGGA	9.389	8.930	6.556
mBJ	9.399	8.945	6.566

respectively. The term $p_{\mathrm{cv}}^{i}(k)$ denotes the momentum matrix element transition from the energy level c of the conduction band to the level v of the valence band at certain **k**-point in the BZ and V is the unit cell volume. Since the LiBe is intermetallic compound, there are two contributions to optical dielectric function: the intra-band (Drude term) and inter-band transitions [30] giving by

$$\varepsilon_2^{ij}(\omega) = \varepsilon_{2\mathrm{intra}}^{ij}(\omega) + \varepsilon_{2\mathrm{inter}}^{ij}(\omega) \tag{3}$$

$$= \frac{\omega_P^{ij}\tau}{\omega(1+\omega^2\tau^2)} + \frac{8\pi^2\hbar^2e^2}{m^2V}\sum_k\sum_{\mathrm{cv}}(f_{\mathrm{c}}-f_{\mathrm{v}})\frac{p_{\mathrm{cv}}^{i}(k)p_{\mathrm{vc}}^{j}(k)}{E_{\mathrm{vc}}^2} \times \delta[E_{\mathrm{c}}(k)-E_{\mathrm{v}}(k)-\hbar\omega] \tag{4}$$

and

$$\omega_{\mathrm{P}}^{ij2} = \frac{8\pi}{3}\sum_{kn}\vartheta_{kn}^{ij2}\delta(\varepsilon_{kn}) \tag{5}$$

where ω_{P} is the anisotropic plasma frequency [31], τ is the mean free time between collisions and ε_{kn} is $E_n(k) - E_{\mathrm{F}}$ and ϑ_{kn}^{ij} is the electron velocity. The values of the plasma frequency are listed in Table 2. The imaginary part of the optical dielectric function is calculated with and without inclusion of the Drude term. We have found that the Drude term has significant effect at energies $\leq$1.0 eV. The sharp rise below 1.0 eV is due to the Drude term. The dispersion of the imaginary part of the optical dielectric function for different incident light polarizations [1 0 0], [1 0 1] and [0 0 1] with respect to the crystalline axes is presented in Fig. 6(a). It is observed that the two polarizations at [1 0 0] and [0 1 0] directions exhibit isotropic behavior at the energy range of 0.0–3.0 and 9.0–12.0 eV, while it shows considerable anisotropy in the energy range of 3.0–9.0 eV. The third polarization [0 0 1] direction shows considerable anisotropy with both [1 0 0] and [0 1 0] polarizations.

The calculated electronic band structure and partial DOS help to analyze the optical transitions that are responsible for the spectral structures in $\varepsilon_2^{xx}(\omega)$, $\varepsilon_2^{yy}(\omega)$ and $\varepsilon_2^{zz}(\omega)$ in accordance with the optical selection rules. In order to identify these spectral structures, we need to look at the magnitude of the optical matrix elements and the angular momentum character of the bands. These spectral structures correspond to the electric-dipole transitions between Li-*s*/*p* and Be-*s*/*p* bands in the valence and conduction bands. The observed spectral structures of $\varepsilon_2^{xx}(\omega)$, $\varepsilon_2^{yy}(\omega)$ and $\varepsilon_2^{zz}(\omega)$ correspond to those transitions that have large optical matrix elements.

These transitions are labeled according to the spectral peak positions in Fig. 6(a). For simplicity, we have labeled the transitions in Fig. 6(a), as A, B and C. The transitions A, B and C are responsible for the structures for $\varepsilon_2^{xx}(\omega)$, $\varepsilon_2^{yy}(\omega)$ and $\varepsilon_2^{zz}(\omega)$ in the spectral ranges of 0.0–4.0, 4.0–8.0 eV and 8.0–12.0 eV, respectively. From the imaginary part of the optical dielectric function, we can obtain the real part using the Kramers–Kronig relations [30]. These are illustrated in Fig. 6(b). It confirms the existence of the considerable anisotropy between $\varepsilon_1^{zz}(\omega)$ and both of $\varepsilon_1^{xx}(\omega)$ and $\varepsilon_1^{yy}(\omega)$.

Using the calculated dispersion of imaginary and real parts of the dielectric function, we have evaluated other optical properties such as reflectivity spectra $R(\omega)$, absorption coefficients $I(\omega)$ and refractive indices $n(\omega)$. Figure 6(c) exhibits the reflectivity spectra of LiBe compound. It is clear that this compound exhibits high reflectivity (unity) at low energies and thereafter drops to form the first reflectivity minima between 4.0 and 8.0 eV confirming the occurrence of a collective plasmon resonance. The depth of the plasmon minimum is determined by the imaginary part of the dielectric function at the plasma resonance and is representative of the degree of overlap between the inter-band absorption regions. The absorption coefficient as illustrated in Fig. 6(d), shows that the investigated compound has zero absorption at low energy ($\leq$1.0 eV) confirming that this compound possesses high reflectivity (unity), thereafter the absorption increase rapidly with increasing the energy of the incident photons. The calculated refractive indices $n^{xx}(\omega)$, $n^{yy}(\omega)$ and $n^{zz}(\omega)$ as represented in Fig. 6(e), exhibits high values of the refractive indices at low energies and thereafter drop to lower values. Again it shows that there exists a considerable anisotropy between $n^{zz}(\omega)$ and the other two components $n^{xx}(\omega)$ and $n^{yy}(\omega)$ along [1 0 0] and [0 1 0] polarization directions.

4. Conclusions

We have relaxed the geometry of LiBe, taken from the X-ray diffraction data of Feng et al. [7] by minimizing the forces acting on each atom and we have assumed that the structure is totally relaxed when the forces on each atom reach values less than 1 mRy/a.u. From the resulting relaxed geometry, we have calculated the ground state properties of the intermetallic LiBe using the all-electron full-potential linearized augmented plane wave within four types of exchange correlations potentials, these are LDA,

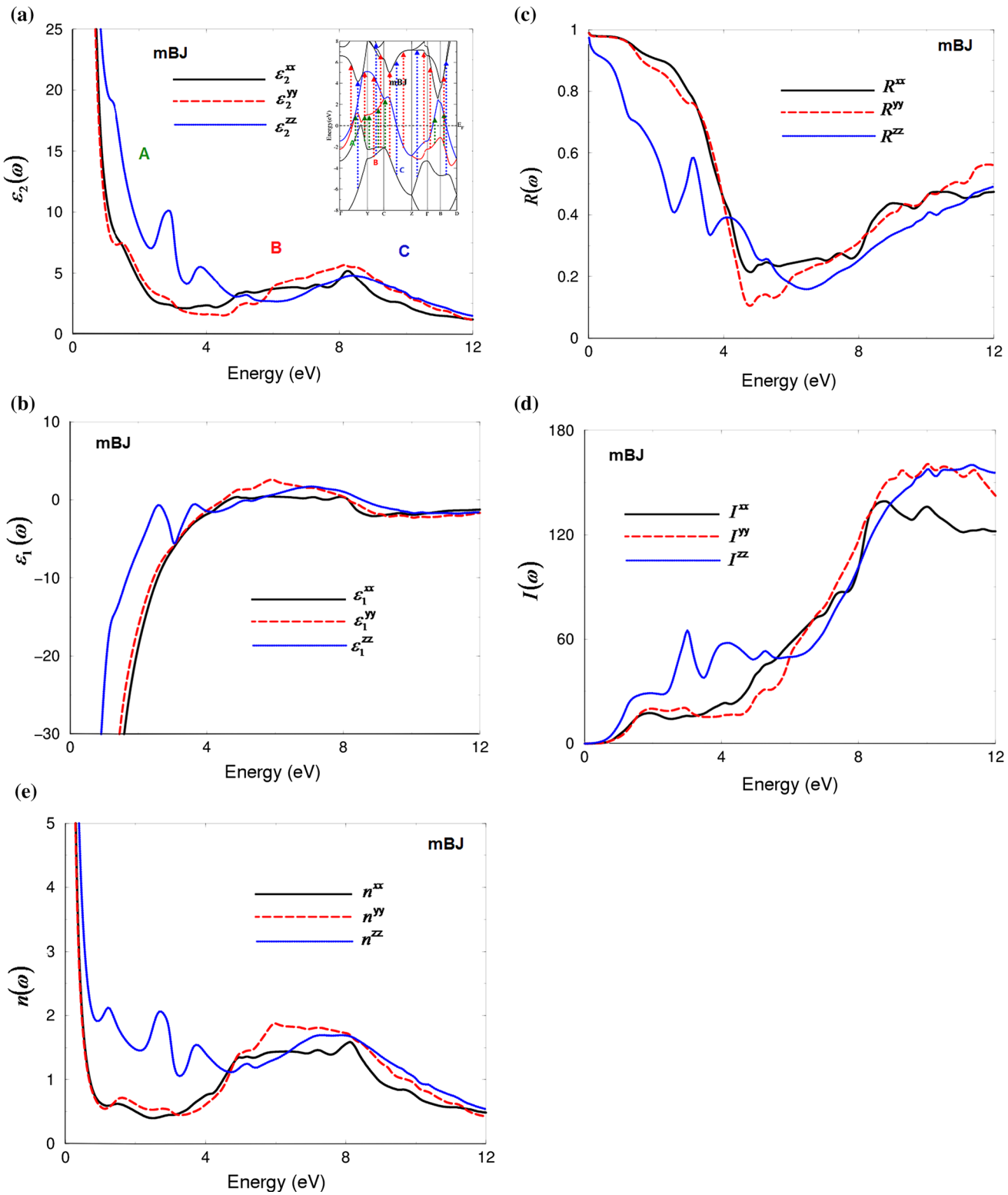

Fig. 6 (**a**) Calculated $\varepsilon_2^{xx}(\omega)$, $\varepsilon_2^{yy}(\omega)$ and $\varepsilon_2^{zz}(\omega)$ (light *solid curve-blue color* online) spectra. (**b**) Calculated $\varepsilon_1^{xx}(\omega)$, $\varepsilon_1^{yy}(\omega)$ and $\varepsilon_1^{zz}(\omega)$ spectra; (**c**) calculated $R^{xx}(\omega)$, $R^{yy}(\omega)$, and $R^{zz}(\omega)$, along with our measured total $R(\omega)$; (**d**) calculated absorption coefficient $I^{xx}(\omega)$, $I^{yy}(\omega)$ and $I^{zz}(\omega)$ spectra. The absorption coefficient in 10^4 s^{-1}; (**e**) calculated refractive indices $n^{xx}(\omega)$, $n^{yy}(\omega)$ and $n^{zz}(\omega)$ spectra

GGA, EVGGA and mBJ. It has been found that moving from LDA → GGA → EVGGA → mBJ shows insignificant influence on the calculated properties. The dispersion of the electronic band structure, total and the angular momentum resolved projected DOS suggest that there exists a strong hybridization between the sates resulting in covalent bonds. The Fermi surface is formed by electrons and holes. The electronic charge density distribution confirms that the charge is attracted toward Be atoms and the calculated bond lengths are in good accord with the available experimental data. The optical properties are investigated and analyzed in accordance with the calculated band structure and the DOS in order to get deep insight into the electronic structure.

Acknowledgments The result was developed within the CENTEM project, Reg. No. CZ.1.05/2.1.00/03.0088, cofunded by the ERDF as part of the Ministry of Education, Youth and Sports OP RDI programme and in the follow-up sustainability stage, supported through CENTEM PLUS (LO1402) by financial means from the Ministry of Education, Youth and Sports under the National Sustainability Programme I. Computational resources were provided by MetaCentrum (LM2010005) and CERIT-SC (CZ.1.05/3.2.00/08.0144) infrastructures.

References

[1] G Das and A C Wahl *Phys. Rev. A* **4** 825 (1971)
[2] W H Fink *J. Chem. Phys.* **57** 1822 (1972)
[3] J Pascale and J Vandeplanque *J. Chem. Phys.* **60** 2278 (1974)
[4] R O Jones *J. Chem. Phys.* **72** 3197 (1980)
[5] Y Xu, C Chen and B Wu *Solid State Commun.* **152** 151 (2012)
[6] K L Galav, U Paliwal and K B Joshi *Comput. Mater. Sci.* **69** 267 (2013)
[7] J Feng, R G Hennig, N W Ashcroft and R Hoffmann *Nat. Lett.* **451** 445 (2008)
[8] I Fischer, V E Bondybey, P Rosmus and H-J Werner *Chem. Phys.* **151** 295 (1991)
[9] L X Ling, H Z Jiang, W X Ming and L Y Hua *Chin. Phys. B* **17** 3687 (2008)
[10] S Gao *Comput. Phys. Commun.* **153** 190 (2003)
[11] K Schwarz *J. Solid State Chem.* **176** 319 (2003)
[12] B I Sharma, J Maibam, R S Paul, R K Thapa and R K B Singh *Indian J. Phys.* **84** 671 (2010)
[13] T Rasheed and S Ahmad *Indian J. Phys.* **85** 239 (2011)
[14] C Pal and R J Kshirsagar *Indian J. Phys*. **84** 929 (2010)
[15] D Sajan, T Kuruvilla, K P Laladhas and I Hubert Joe *Indian J. Phys.* **85** 477 (2011)
[16] P Blaha, K Schwarz, G K H Madsen, D Kvasnicka and J Luitz *WIEN2k, An augmented plane wave plus local orbitals program for calculating crystal properties* (Austria: Vienna University of Technology) (2001)
[17] J P Perdew, S Burke and M Ernzerhof *Phys. Rev. Lett.* **77** 3865 (1996)
[18] W Kohn and L J Sham *Phys. Rev. A* **140** 1133 (1965)
[19] E Engel and S H Vosko *Phys. Rev. B* **47** 13164 (1993)
[20] F Tran and P Blaha *Phys. Rev. Lett.* **102** 226401 (2009)
[21] W Setyawan and S Curtarolo *Comp. Mat. Sci.* **49** 299 (2010)
[22] A H Reshak *Phys. Chem. Chem. Phys*. **16** 10558 (2014)
[23] A H Reshak, V Kityk, O V Parasyuk, H Kamarudin and S Auluck *J. Phys. Chem. B* **117** 2545 (2013)
[24] A H Reshak, Z A Alahmed and S Auluck *Solid State Sci.* **38** 138 (2014)
[25] A H Reshak and S Auluck *Opt. Mater.* **38** 80 (2014)
[26] R Schlachta, I Fischer, P Rosmus and V E Bondybey *Chem. Phys. Lett.* **170** 485 (1990)
[27] A I Boldyrev, J Simons and Paul von F L Schleyer *J. Chem. Phys.* **99** 8793 (1993)
[28] C W Bauschlicher, Jr, S R Langhoff and H Partidge *J. Chem. Phys.* **96** 1240 (1992)
[29] F Bassani and G P Parravicini *Electronic States and Optical Transitions in Solids* (UK: Pergamon Press Ltd Oxford) p 149 (1975)
[30] F Wooten *Optical Properties of Solids* (USA: Academic press New York) (1972)
[31] M I Kolinko, I V Kityk and A S Krochuk *J. Phys. Chem.* **53** 1315 (1992)